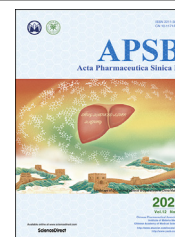




Chinese Pharmaceutical Association
Institute of Materia Medica, Chinese Academy of Medical Sciences

Acta Pharmaceutica Sinica B

www.elsevier.com/locate/apsb
www.sciencedirect.com



ORIGINAL ARTICLE

Novel phthalimides regulating PD-1/PD-L1 interaction as potential immunotherapy agents



Chengliang Sun^{a,b,†}, Yao Cheng^{a,c,†}, Xiaojia Liu^{d,†}, Gefei Wang^{a,b},
Wenjian Min^{a,b}, Xiao Wang^{a,b}, Kai Yuan^{a,b}, Yi Hou^{a,b}, Jiaxing Li^{a,b},
Haolin Zhang^{a,b}, Haojie Dong^{a,b}, Liping Wang^{a,b}, Chenguang Lou^e,
Yanze Sun^{a,b}, Xinmiao Yu^{a,b}, Hongbin Deng^{f,*}, Yibei Xiao^{a,c,*},
Peng Yang^{a,b,*}

^aState Key Laboratory of Natural Medicines and Jiangsu Key Laboratory of Drug Design and Optimization, China Pharmaceutical University, Nanjing 210009, China

^bDepartment of Medicinal Chemistry, School of Pharmacy, China Pharmaceutical University, Nanjing 211198, China

^cDepartment of Pharmacology, School of Pharmacy, China Pharmaceutical University, Nanjing 211198, China

^dBeijing Institute of Clinical Pharmacy, Beijing Friendship Hospital, Capital Medical University, Beijing 100050, China

^eDepartment of Physics, Chemistry and Pharmacy, University of Southern Denmark, Campusvej 55, 5230 Odense, Denmark

^fInstitute of Medicinal Biotechnology, Chinese Academy of Medical Sciences & Peking Union Medical College, Beijing 100050, China

Received 28 January 2021; received in revised form 30 March 2021; accepted 6 April 2022

KEY WORDS

PD-1/PD-L1;
Small-molecule inhibitor;
Immunotherapy;
Co-crystal structure

Abstract Programmed cell death 1(PD-1)/programmed cell death ligand 1(PD-L1) have emerged as one of the most promising immune checkpoint targets for cancer immunotherapy. Despite the inherent advantages of small-molecule inhibitors over antibodies, the discovery of small-molecule inhibitors has fallen behind that of antibody drugs. Based on docking studies between small molecule inhibitor and PD-L1 protein, changing the chemical linker of inhibitor from a flexible chain to an aromatic ring may improve its binding capacity to PD-L1 protein, which was not reported before. A series of novel phthalimide derivatives from structure-based rational design was synthesized. **P39** was identified as the best inhibitor with promising activity, which not only inhibited PD-1/PD-L1 interaction

*Corresponding authors.

E-mail addresses: hdeng@imb.pumc.edu.cn (Hongbin Deng), yibei.xiao@cpu.edu.cn (Yibei Xiao), pengyang@cpu.edu.cn (Peng Yang).

†These authors made equal contributions to this work.

Peer review under responsibility of Chinese Pharmaceutical Association and Institute of Materia Medica, Chinese Academy of Medical Sciences.

<https://doi.org/10.1016/j.apsb.2022.04.007>

2211-3835 © 2022 Chinese Pharmaceutical Association and Institute of Materia Medica, Chinese Academy of Medical Sciences. Production and hosting by Elsevier B.V. This is an open access article under the CC BY-NC-ND license (<http://creativecommons.org/licenses/by-nc-nd/4.0/>).

($IC_{50} = 8.9$ nmol/L), but also enhanced killing efficacy of immune cells on cancer cells. Co-crystal data demonstrated that **P39** induced the dimerization of PD-L1 proteins, thereby blocking the binding of PD-1/PD-L1. Moreover, **P39** exhibited a favorable safety profile with a $LD_{50} > 5000$ mg/kg and showed significant *in vivo* antitumor activity through promoting $CD8^+$ T cell activation. All these data suggest that **P39** acts as a promising small chemical inhibitor against the PD-1/PD-L1 axis and has the potential to improve the immunotherapy efficacy of T-cells.

© 2022 Chinese Pharmaceutical Association and Institute of Materia Medica, Chinese Academy of Medical Sciences. Production and hosting by Elsevier B.V. This is an open access article under the CC BY-NC-ND license (<http://creativecommons.org/licenses/by-nc-nd/4.0/>).

1. Introduction

After decades of development, immunotherapy regimens have been gradually refined, and in recent years, one of the most rapidly developing treatment regimens is PD-1/PD-L1 therapy^{1–4}. Immune checkpoints are a series of molecules that are expressed on immune cells and can regulate the activation degree of immune cells. They play an important role in combating autoimmunity and suppressing excessive activation of immune cells, and PD-1/PD-L1 is one of the most important checkpoint molecules^{5,6}. PD-1/PD-L1 regulates the immune system and promotes self-tolerance by down-regulating the immune system's response to human cells and by suppressing T-cell inflammatory activity^{5,7}. Tumor cells can express PD-L1 and achieve immune escape through this mechanism to avoid being killed by T cells⁸. By inhibiting the PD-1/PD-L1 axis, the ability of T cells to attack tumor cells can be restored to cure cancer⁹.

There are 4 PD-1 antibodies (pembrolizumab, nivolumab, cemiplimab, dostarlimab) and 3 PD-L1 antibodies (avelumab, atezolizumab, durvalumab) approved by U.S. Food and Drug Administration (FDA) for clinical applications¹⁰. As an example, the approved indications of pembrolizumab have been increased to 18 types of cancer including and not limited to non-small cell lung cancer, classical Hodgkin lymphoma, head, and neck squamous cell carcinoma, primary mediastinal large B-cell lymphoma¹¹. Global sales of pembrolizumab and nivolumab reached \$14.38 billion and \$7.92 billion respectively in 2020. However, antibody drugs have some natural drawbacks, such as poor oral bioavailability, poor permeability of tumor tissues, immune-related adverse events, and high medical costs^{12,13}. One improving strategy is to investigate small molecule PD-L1

inhibitors. After several antibody drugs came to market and showed good efficacy, small molecule PD-1/PD-L1 inhibitors had become a hot research topic.

In the past few years, there have been some important advances in this area. The Bristol-Myers Squibb company has discovered a series of biphenyl derivatives^{14,15} that can lead to dimerization of PD-L1 molecules. Holak's group^{16,17} has disclosed the co-crystal structures of the complex which provides a very good research basis for subsequent small molecule inhibitor studies. A large number of companies and research institutions are involved in developing novel PD-1/PD-L1 small molecule inhibitors^{11,13–15,18–27} (Fig. 1), but the vast majority of small molecules are still in preclinical studies. This indicates that druggable small molecule inhibitors are still to be discovered and further exploration is needed to find small molecule inhibitors for clinical use.

In this study, we designed and synthesized novel phthalimide derivatives as small-molecule inhibitors against the PD-1/PD-L1 pathway. Their structure–activity relationships were systematically evaluated, and **P39** was identified as the most promising leading compound with an IC_{50} value of 8.9 nmol/L which was assessed by a TR-FRET assay. **P39** reduced the PD-1/PD-L1 interaction and enhanced the cytotoxicity of PBMCs against cancer cells in a dose-dependent manner. **P39** also showed outstanding *in vivo* antitumor activity in a MC38 mouse model and a humanized LLC-hPD-L1 tumor model, which was worthy of further evaluation. Notably, this study identified the possibility of replacing flexible chains with aromatic rings as the linker in PD-1/PD-L1 inhibitors, which was verified by crystal structure and would well guide the subsequent exploration of potential drugs using aromatic rings as the linker.

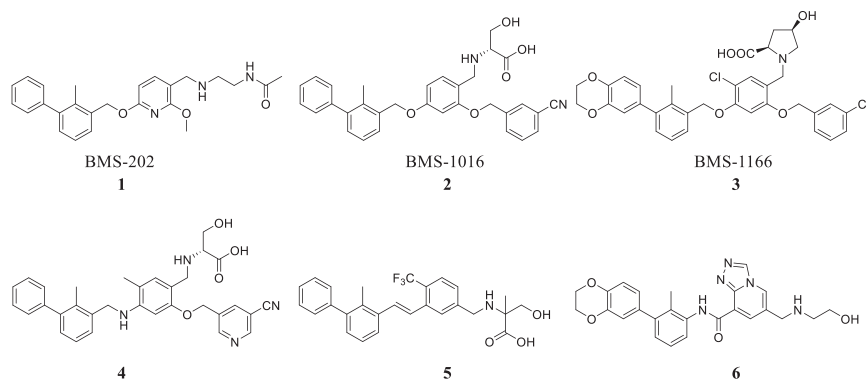


Figure 1 Structures of representative small-molecule inhibitors of PD-1/PD-L1.

2. Results and discussion

2.1. Drug design

Crystal structure of human PD-1/PD-L1 complex was first reported by Holak in 2015¹⁶. Three hot spots were recommended and key amino acid residues on the interaction surface of the complexes were disclosed, which included Tyr 56, Glu 58, Arg 113, Met 115, Ala 121, and Tyr 123 on PD-L1. Moreover, this research group determined the co-crystal structure of PD-L1 dimer by using a small molecule (BMS202). It could be found that the binding surface of the PD-L1 dimer (Fig. 2A and B) is overlapping with the PD-1/PD-L1 binding surface¹⁷. This is the mechanism of how BMS202 inhibits PD-1/PD-L1 protein–protein interactions.

It is known from the data of molecular docking that biphenyl moiety is necessary for maintaining inhibitory activity¹⁷ (Fig. 2D). Ring A would form a T-stacking interaction with the residue _ATyr 56, and further stabilized by the sidechains of _BAla 121 and _AMet 115 through π -alkyl interactions, and the ring B creates a hydrophobic interaction with _AAla 121 and _BMet 115. The pyridine ring is involved in π - π stacking with _BTyr 56. These substituents are presumed to be important for maintaining activity and appear in almost all reported small molecules. Ethers are commonly chosen as the linkers and play a limited role in SARs. Replacing the ether linker with a better moiety could create more interactions and is the desired strategy. The co-crystal structure of PD-L1/BMS202 was further analyzed. _BTyr 56 would be able to form a π - π stacking with the linker if replace the linker from the ether moiety into an aromatic ring.

Based on this rational-design strategy, a series of phthalimide derivatives were designed and the docking results were consistent with expectations (Fig. 2E). The molecule docking showed that the newly designed molecule not only retains all the hydrophobic bonds formed by BMS202 with the dimer cavity after replacing the ether bond with the phthalimide ring but also forms strong π -

π stacking with _BTyr 56, supporting the correctness of our rational-design strategy.

2.2. Chemistry

To verify the PD-1/PD-L1 inhibitory activity of designed molecules, a series of phthalimide derivatives were synthesized. The synthesis of phthalimide derivatives **P1–P8**, **P11–P16**, **P18–P41** are described in Schemes 1 and 2. Suzuki-Miyaura coupling of compounds **7a–d** with phenylboronic acid yielded intermediates **8a–d**, respectively. Using acetic acid as the solvent, compounds **8a–d** reacted with 4-hydroxyphthalic acid to yield intermediates **9a–d**. Compounds **9a–d** reacted with hexamethylenetetramine to yield intermediates **10a–d** through a Duff reaction. The etherification of intermediates **10a–d** with the appropriate benzyl bromides provided the intermediates **11a–h**, followed by NaBH(OAc)₃-mediated reductive amination with an appropriate amine to yield the final compounds **P1**, **P3–P8**, **P11–P16**, **P18–P41**. While for target compound **P2**, intermediate **10a** directly reacted with ethanolamine to yield the product.

The synthesis of phthalimide derivatives **P9–P10** is described in Scheme 3. Intermediate **12** is a by-product of the reaction that produces intermediate **10a** (Scheme 2). Similar to the design of compounds **P7–P8**, **P11–P16**, and **P18–P41**, we conducted a two-step reaction and obtained the target products **P9–P10** to investigate the structure–activity relationship of the R₄ substituent.

The synthesis of target compound **P17** is described in Scheme 4. The Suzuki-Miyaura coupling reaction between **7a** and phenylboronic acid derivatives provided biphenyl compound **14**. Using acetic acid as the solvent, compound **14** reacted with 5-hydroxybenzene-1,2,4-tricarboxylic acid to yield intermediate **15**. Followed by reduction and oxidation to yield intermediates **16** and **17**. Finally, compound **P17** was prepared according to the similar procedure of compound **P1** in two steps.

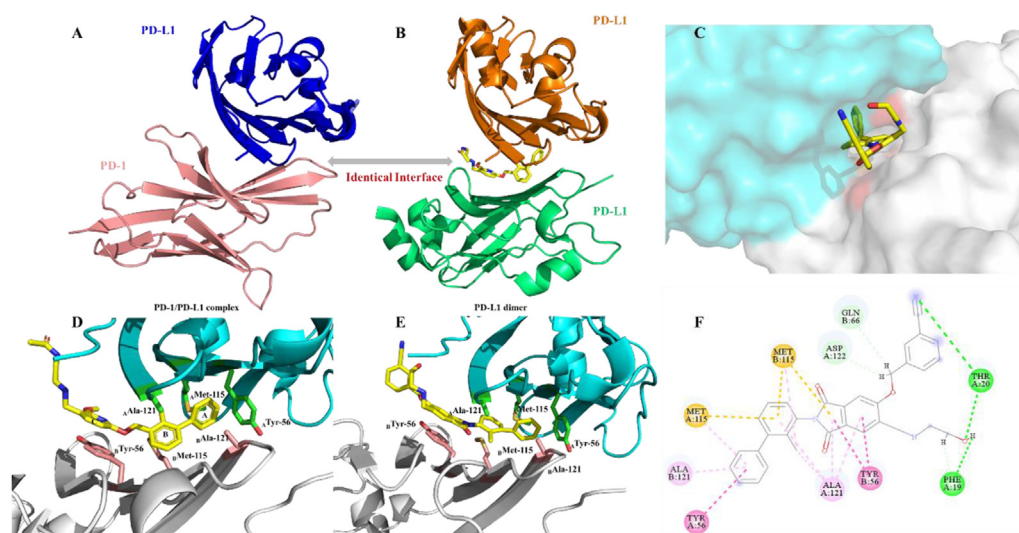
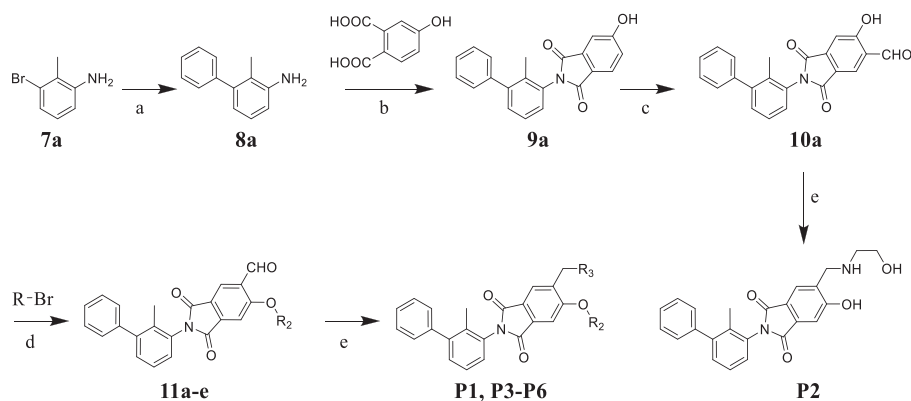
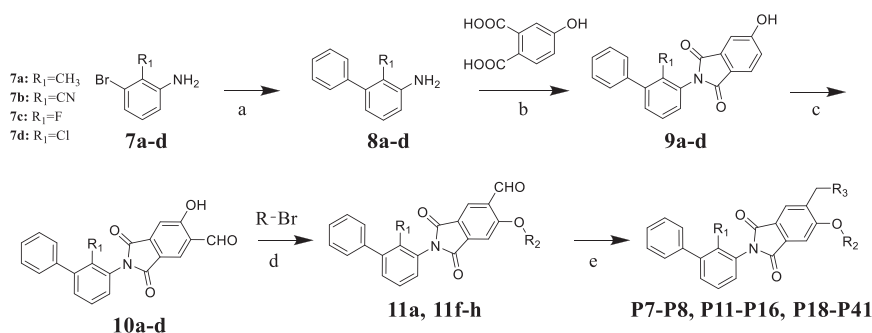


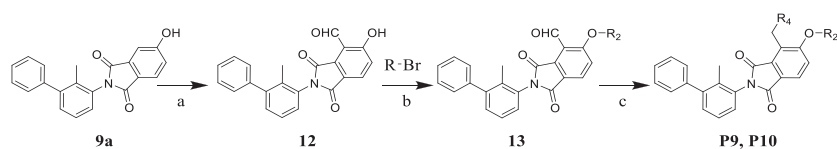
Figure 2 Mechanism of PD-1/PD-L1 complex formation inhibition by small molecule inhibitor. (A) PD-1/PD-L1 interaction (PD-1 shown as the pink cartoon, PD-L1 shown as the blue cartoon, PDB: 4ZQK¹⁶). (B) BMS202 (yellow) induced dimerization of PD-L1 (orange, PD-L1; green, PD-L1; PDB: 5J89¹⁷). (C) Docking analysis of newly designed leading compound **P1** (3D model, cyan, model A; grey, model B). (D) Co-crystal structure of BMS202 and PD-L1 dimer (cyan, model A; grey, model B; PDB: 5J89). (E) Docking analysis of newly designed leading compound **P1** (3D model, cyan, model A; grey, model B). (F) Binding conformation of the leading compound **P1** in PD-L1/PD-L1 dimer. The π - π stacking interactions were shown as a red dash line, and hydrogen-bonding interactions were shown as a green dash line.



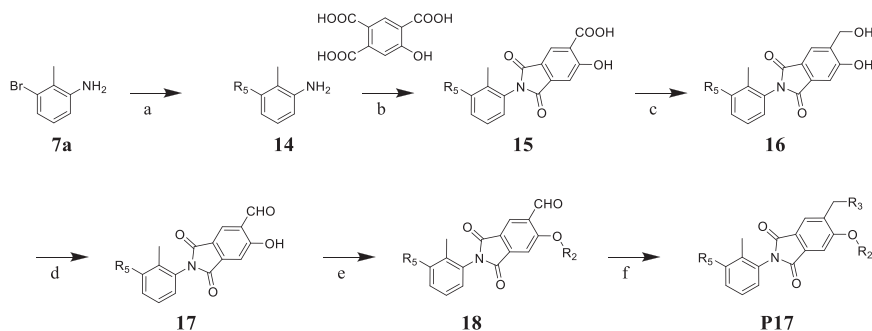
Scheme 1 Synthesis of compounds **P1–P6**. Reagents and condition: (a) phenylboronic acid, Pd(OAc)₂, K₂CO₃, EtOH/H₂O (1:1), rt, 14 h, 82%; (b) AcOH, 120 °C, 7 h, 83%; (c) hexamethylenetetramine, CF₃COOH, 120 °C, 10 h, 35%; (d) DMF, Cs₂CO₃, 80 °C, 2 h, 76%–80%; (e) appropriate amine, NaBH(OAc)₃, CH₂Cl₂, rt, 6–10 h, 21%–30%.



Scheme 2 Synthesis of compounds **P7–P8**, **P11–P16**, and **P18–P41**. Reagents and condition: (a) phenylboronic acid, Pd(OAc)₂, K₂CO₃, EtOH/H₂O (1:1), rt, 14 h, 79%–82%; (b) AcOH, 120 °C, 7 h, 79%–83%; (c) hexamethylenetetramine, CF₃COOH, 120 °C, 10 h, 30%–35%; (d) DMF, Cs₂CO₃, 80 °C, 2 h, 77%–80%; (e) appropriate amine, NaBH(OAc)₃, CH₂Cl₂, rt, 6–10 h, 21%–69%.



Scheme 3 Synthesis of compounds **P9–P10**. Reagents and condition: (a) hexamethylenetetramine, CF₃COOH, 120 °C, 10 h, 10%; (b) DMF, Cs₂CO₃, 80 °C, 2 h, 75%; (c) appropriate amine, NaBH(OAc)₃, CH₂Cl₂, rt, 6–10 h, 40%–55%.



Scheme 4 Synthesis of compounds **P41**. Reagents and condition: (a) phenylboronic acid derivatives, Pd(OAc)₂, K₂CO₃, EtOH/H₂O (1:1), rt, 14 h, 84%; (b) AcOH, 120 °C, 7 h, 72%; (c) BH₃·THF, THF, 10 h, rt, 70%; (d) Dess-Martin periodane, CH₂Cl₂, rt, 2 h, 75%; (e) DMF, Cs₂CO₃, 80 °C, 2 h, 80%; (f) appropriate amine, NaBH(OAc)₃, CH₂Cl₂, rt, 10 h, 52%.

2.3. Biochemical evaluation and structural optimization

For all the final compounds, the inhibitory activities regulating the PD-1/PD-L1 interactions were evaluated using TR-FRET method.

To verify the effect of the R₂ substituent on activity, new derivatives **P1–P6** were designed and further synthesized, and the IC₅₀ values were shown in Table 1 and BMS202 was tested as the positive compound. All six derivatives used ethanolamine as the hydrophilic tail. Based on the docking results between PD-L1 and leading compound **P1** in Fig. 2F, the 3-cyanobenzyl group in **P1** formed a strong hydrogen bond interaction with the residue _AThr 20. To confirm the importance of the 3-cyanobenzyl group as a R₃ substituent, we firstly removed it directly and synthesized compound **P2**. The results indicated that the inhibitory activity of compound **P2** was dramatically decreased, which elucidated the important role of the 3-cyanobenzyl substituent. Furthermore, we changed the cyano position on the benzyl ring and synthesized **P3–P4** to explore the influence of the substituent position on the activity. The *meta*-substituted compound **P1** showed the best activity (**P1**: IC₅₀ = 45.4 nmol/L), while the *ortho*- and *para*-substituted compounds **P3** and **P4** only showed moderate activities (**P3**: IC₅₀ = 170.9 nmol/L, and **P4**: IC₅₀ = 153.1 nmol/L). Meanwhile, if we removed the cyano substituent to get compound **P5**, its activity was similar to **P3** and **P4**. Also, if we replaced the *para*-cyano group of compound **P4** with a 4-isopropylbenzyl group, its inhibitory activity decreased six folders. All these results indicate that the 3-cyanobenzyl used in compound **P1** is the optimal substituent, which will be kept for further modification.

Both the docking study and above SAR results indicate that introduction of the R₃ substituent at the 5-position is the preferred design strategy. However, we obtained the intermediate **12** as a by-product during the synthesis of intermediate **10a** (Schemes 2 and 3). Therefore, we could obtain target compounds **P7** and **P8** with 3-R₄ substituent instead of 5-R₃ at ring C, and the IC₅₀ values were shown in Table 2. Comparing compounds **P7/8** with **P9/10**, the position change of the R₃ substituent caused a significant decrease in the activity (**P7**: IC₅₀ = 45.6 nmol/L vs **P9**: IC₅₀ = 1141.0 nmol/L), which verifies that the strategy of our rational design is correct. Therefore, we will maintain the 5-R₃ substituent in further modification.

After exploring the influence of R₃ on ring C, we further investigated the effect of R₁ on ring B (Table 3). The methyl substituent on ring B was modified to a cyano, fluorine, or chlorine

Table 1 PD-1/PD-L1 inhibitory activity of compounds **P1–P6**.

Compd.	R ₂	IC ₅₀ (nmol/L)
P1		45.4
P2	H	739.4
P3		170.9
P4		153.1
P5		216.4
P6		920.7
BMS202		17.0

Table 2 PD-1/PD-L1 inhibitory activity of compounds **P7–P10**.

Compd.	R ₃	R ₄	IC ₅₀ (nmol/L)
P7		/	45.6
P8		/	52.1
P9	/		1141.0
P10	/		4382.0
BMS202			17.0

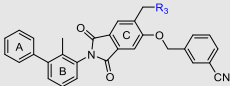
group. Interestingly, all the final compounds showed slightly improved activity (Tables 2 and 3: **P11** vs **P12**, **P8** vs **P14** vs **P16**). Although fluoro- or chloro-substituted compounds **P16** and **P14** showed a little better activity, raw material for methyl-substituted products is the most accessible. Therefore, methyl substituent was selected for the follow-up studies.

Besides keeping R₅ as a phenyl ring, R₅ was also replaced by a heterocycle benzodioxane group. Although this strategy led to a slightly decreased activity, the inhibitory activity of these two compounds (**P7**: 45.6 nmol/L vs **P17**: 50.4 nmol/L) was still at the same level and the synthesis of phenyl derivatization **P7** was easier. Therefore, we kept R₅ as a phenyl substituent for further modification. Of course, the heterocycle benzodioxane group may be a good direction to improve the physicochemical properties of the target compounds in future studies.

As shown in Table 3, the hydrophilic R₃ tail was reported to play an important role in binding with PD-L1 and serve as hydrogen-bond donors^{21,23}. To further investigate the diversity of hydrophilic substituents R₃, a series of new derivatives with a chain or cyclic hydrophilic tail were designed and synthesized, including ester groups, alcohol groups, amide groups, and carboxyl groups (Table 4). Among these newly designed compounds, **P22–P27** bearing a cyclic substituent showed weaker

Table 3 PD-1/PD-L1 inhibitory activity of compounds **P11–P17**.

Compd.	R ₁	R ₃	R ₅	IC ₅₀ (nmol/L)
P11	CH ₃			117.5
P12	CN			100.0
P13	Cl			39.3
P14	Cl			22.1
P15	F			58.7
P16	F			31.6
P17	CH ₃			50.4
BMS202				17.0

Table 4 PD-1/PD-L1 inhibitory activity of compounds **P18–P41**.


Compd.	R ₃	IC ₅₀ (nmol/L)	Compd.	R ₃	IC ₅₀ (nmol/L)
P18		79.1	P31		835.8
P19		150.4	P32		1155.0
P20		395.4	P33		13.3
P21		188.9	P34		>10,000
P22		250.7	P35		46.6
P23		216.1	P36		1667.0
P24		738.1	P37		11.6
P25		187.4	P38		>10,000
P26		563.7	P39		8.9
P27		42.4	P40		1686.0
P28		867.4	P41		527.1
P29		607.0	BMS202		17.0
P30		14.0			

activities when compared with compounds **P18–P21** with a chain tail. This indicates that a R₃ chain tail may be a better choice for further modification. Meanwhile, replacing the hydroxyl group with a carboxyl group greatly improved the activity (**P25** vs **P27**). Therefore, we further introduced the chain tail with a carboxyl group into the new derivatives and explored their structure-activity relationship. This strategy offered us a series of new compounds (**P30**, **P33**, **P35**, **P37**, and **P39**), which exhibited activities of great improvements. Especially, compound **P39** exhibited the best IC₅₀ value of 8.9 nmol/L. While we converted the carboxyl acid group to different ester groups (**P31**, **P32**, **P34**, **P36**, **P38**, and **P40**), their activities were remarkably decreased. This result further confirmed that the carboxyl acid group played a critical role to maintain the favorable activity.

2.4. Cytotoxicity evaluation

When developing a small molecule PD-L1 immuno-oncology agent, we hope that its inhibitory activity on cancer cells is derived from the regulation of T-cell function rather than the cytotoxicity of the inhibitor. To evaluate the cytotoxicity of these new compounds, 10 representative compounds (**P1**, **P3**, **P4**, **P8**, **P15**, **P17**, **P30**, **P33**, **P37**, and **P39**) were chosen and tested using the Real-Time Cell Analyzing (RTCA) method. A375 cells were treated with 20 μmol/L of the selected compound. As illustrated in Fig. 3A and Supporting Information Fig. S1, real-time growth of A375 cells was measured and found to be almost identical

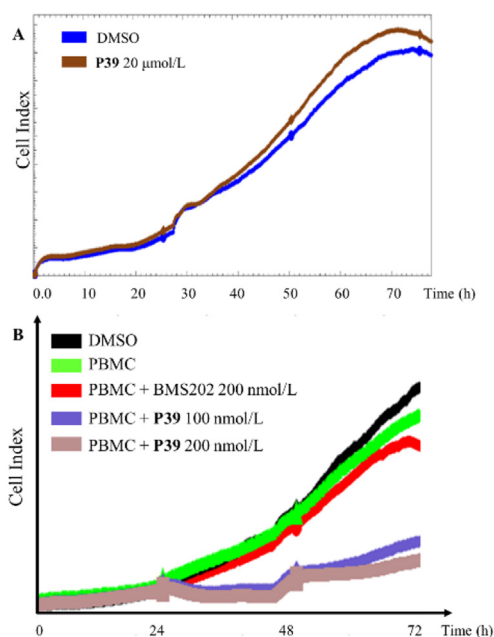


Figure 3 Cytotoxicity effect of **P39** on tumor cell and killing effect of human PBMCs toward H460 cells. (A) Treated with different concentrations of **P39**, cell viability in A375 cells was measured using the xCELLigence system. (B) Cell impedance test was used to examine the killing effects of human PBMCs on H460 cells after treated with **P39** (100 or 200 nmol/L) for 24 h.

between the experimental and control groups, demonstrating that these compounds were essentially non-toxic to A375 cells. Therefore, the cytotoxicity effects can be excluded in the subsequent cellular assays and *in vivo* antitumor experiments.

2.5. Binding affinity of **P39** to PD-L1

Considering the inhibitory action of PD-1/PD-L1 and cellular cytotoxicity, compound **P39** was chosen as the top candidate and its binding affinity to hPD-L1 was further analyzed using micro-scale thermophoresis (MST) method. As shown in Supporting Information Fig. S3, the K_D value for compound **P39** binding to hPD-L1 was 24.4 ± 0.02 nmol/L, while the K_D value for positive control compound BMS202 was 134.8 ± 0.10 nmol/L. It indicated that compound **P39** exhibited a strong binding affinity with human PD-L1 protein than BMS202.

2.6. **P39** reduces PD-1/PD-L1 interaction and increases PBMC cytotoxicity

Based on the above experimental results, compound **P39** was shown to have a high affinity for PD-L1 protein and blocked the protein interaction of PD-1/PD-L1. To assess its inhibitory activity on tumor cells, further cellular assays were performed. It was established that PD-L1 on tumor cells would bind to the homologous receptor PD-1 on tumor-infiltrating T cells thus inhibiting their antitumor activity²⁸. To confirm whether **P39** would influence the protein interaction of PD-1 and PD-L1, tumor cells pretreated with **P39** were cultivated with recombinant human PD-1 Fc. A diminished fluorescent signal indicates the decreased interaction between PD-1 and PD-L1²⁹. It was found that the binding capacity of PD-1 to H460 cells and MDA-MB-231 cells

was significantly decreased in a dose-dependent manner after treatment with **P39**. At a concentration of 200 nmol/L, compound **P39** showed a stronger inhibitory activity compared to the positive compound BMS202 (Fig. 4A and B). Moreover, PD-1/PD-L1 blockade bioassay³⁰ (Fig. 4C and D) also showed the significant increase of transcriptional-mediated bioluminescent signal in **P39**-treated H358 cells in a concentration-dependent manner compared to untreated cells. A549 cells with very low PD-L1 expression served as a positive control. Luciferase signal increases when the protein interaction of PD-1/PD-L1 is blocked. These results suggested that **P39** could block the interaction of PD-1/PD-L1, thereby inhibiting the checkpoint activity of PD-L1.

Furthermore, cell impedance assay was used to evaluate the cytotoxicity of activated human PBMCs against co-cultured cancer cells. Consistently, **P39** greatly increased the sensitivity of tumor cells to T cell killing, and showed a stronger killing ability compare to the BMS202 group (Fig. 3B). In conclusion, all these results suggest that **P39** blocked the interaction of PD-1/PD-L1 and improved the immune killing ability of PBMCs against cancer cells.

2.7. Structural basis for the interaction between **P39** and PD-L1 protein

Crystals of the PD-L1/**P39** complex diffracted to 2.7 Å resolution (Supporting Information Table S1). The asymmetric unit contains eight molecules of PD-L1. Six molecules form three dimers and the other two molecules form two dimers with molecules from neighboring asymmetric unit, respectively (Fig. 5A). The interface of each dimer contains one inhibitor, which forms a cylindrical hydrophobic pocket (Fig. 5B and C). This interaction mode of PD-L1 with **P39** is in high agreement with the previous computer-aided drug design (CADD) results, and all hydrophobic bond

formation is consistent with the calculated results. The ring A of compound **P39** forms T-stacking interactions with the side chain _CTyr 56 and additional π - δ and π -alkyl interactions with _EAla 121 and _CMet 115, respectively. Ring B is stabilized by hydrophobic interactions with _CAla 121 and _EMet 115. Both ring C and the phthalimide ring form π - π stacking with _ETyr 56, which is consistent with the computational design. By adding the phthalimide ring, the small molecule inhibitor forms a stronger hydrophobic interaction with the PD-L1 dimer, which helps stabilize the binding of the inhibitor to the dimer. In addition, 3-cyanobenzyl in the tail of **P39** forms π -cation interaction with _CArg 125. The tails of compound **P39** form a hydrogen bond with _CAsp 122, _CLys 124, and _ETry 56, respectively, which greatly enhances the interaction of the inhibitor with the PD-L1 dimer (Fig. 5E).

Comparison of the co-crystal structures of PD-L1/**P39** complex and PD-L1/BMS202 complex (PDB ID: 5J89) revealed no significant displacement of key amino acid residues for the interaction of the two inhibitors and PD-L1 dimer (Fig. 5D), which suggested that changing the linker chain from a flexible chain to an aromatic heterocyclic may not result in significant change in protein conformation.

2.8. In vivo antitumor activity of compound **P39**

Prior to the *in vivo* efficacy evaluation experiments, acute toxicity experiments and pharmacokinetic (PK) experiments were performed to assess the safety properties of **P39** and to define the appropriate mode of administration. Oral administration of **P39** at a single dose of 5000 mg/kg for two weeks showed no mortality and obvious body weight loss, which proved that compound **P39** had a favorable safety profile (Supporting Information Fig. S4). We evaluated the PK properties of **P39** using SD rats, which showed hopeful PK properties included acceptable $t_{1/2}$ and AUC by

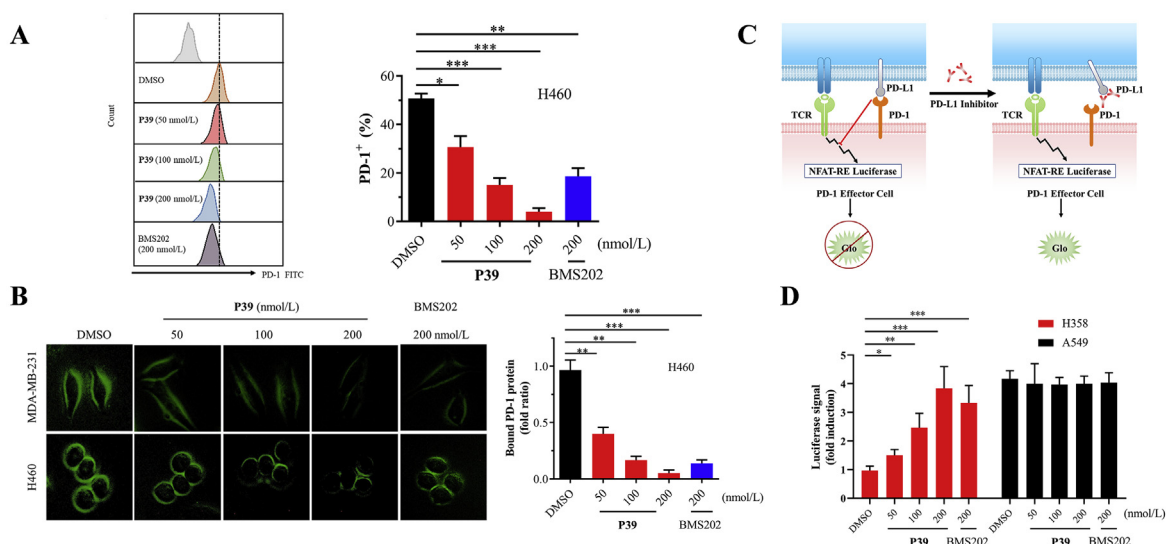


Figure 4 **P39** attenuates PD-1/PD-L1 interaction and strengthens the cytotoxicity of PBMCs. (A) Binding of PD-1 to H460 cells, which were treated with the indicated dose of **P39** for 24 h, was measured by flow cytometry. The Y-axis shows the mean fluorescence intensity of PD-1. (B) After treatment with **P39** (0–200 nmol/L, 24 h) on the MDA-MB-231 and H460 cells, the changes in immunostaining were monitored. The green fluorescence intensity indicates the binding of PD-1 to tumor cells. (C) Addition anti-PD-L1 inhibitor that interfered with the PD-1/PD-L1 interaction results in NFAT-RE-mediated luminescence. (D) Interaction of PD-1/PD-L1 between Jurkat NFAT-luciferase reporter cells and **P39**-treated A549 or H358 cells were measured using the PD-1/PD-L1 blockade assay. Data are shown as fold induction compared to untreated controls.

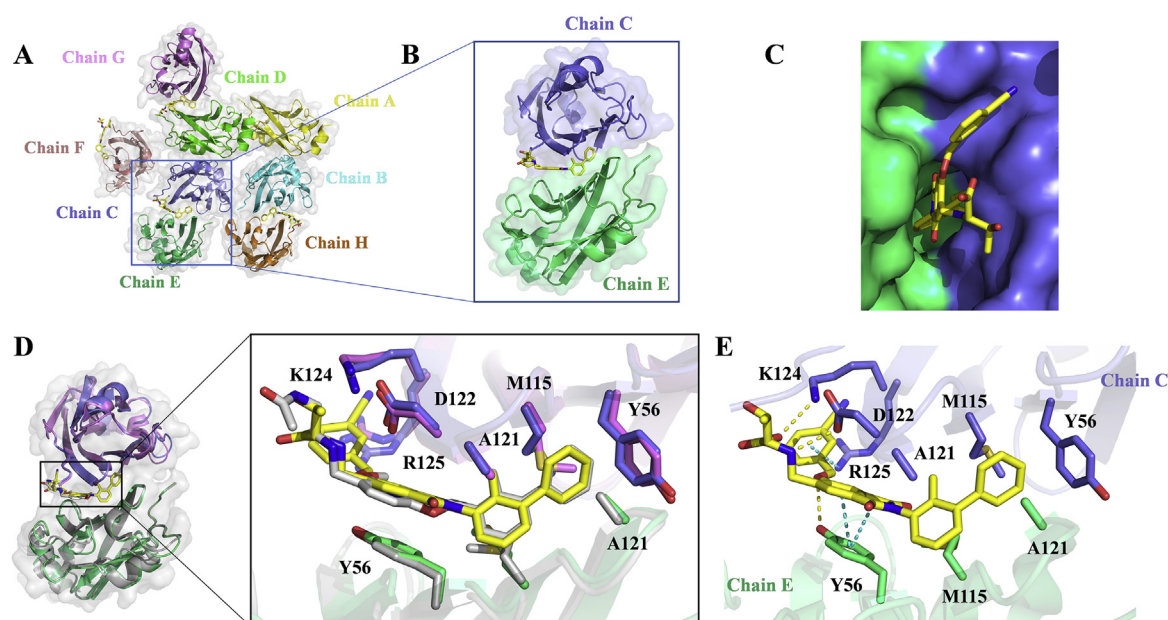


Figure 5 Co-crystal structure of PD-L1/**P39** complex. (A) Each asymmetric unit contains eight PD-L1 molecules (mixed ribbon/surface representation). Six molecules form three dimers and the other two molecules form two dimers with molecules from the other unit, respectively. (B) Structure of a single dimer, color coding as in Fig. 5A. (C) The small-molecule inhibitor **P39** is embedded in a hydrophobic cavity formed by the PD-L1 dimer. (D) Overlay of the PD-L1/**P39** and PD-L1/BMS202 dimer (PDB ID: 5J89). Both **P39** (yellow) and BMS202 (gray) induce the PD-L1 dimerization and form a similar binding pocket (PD-L1/**P39** complex: slate and green, PD-L1/BMS202 complex: violet and gray). (E) Detailed interaction of the inhibitor **P39** with key amino acid residues of the PD-L1 dimer.

injectable administration (Supporting Information Table S2). However, the low oral bioavailability ($F\%$) was similar to the reported compounds. These results guided us to use intraperitoneal injection for the *in vivo* evaluation, while not oral administration. A MC38 mouse model in C57BL/6 mice was used to assess the *in vivo* antitumor efficacy of top compound **P39**. After the tumor volume reached 100 mm^3 , the mice were divided equally into three groups, a blank control group and two experimental groups (dosages: 10 and 25 mg/kg). Compound **P39** was administered by intraperitoneal injection once daily for 4 weeks. The tumor growth inhibition of the different groups was shown in Fig. S5A. Compound **P39** inhibited tumor growth in a dose-dependent manner. After 4 weeks of administration with a low and high dosage of **P39**, the tumor volume growth inhibition was 54.9% and 68.3%, respectively (Supporting Information Fig. S5C). No weight loss or death of mice occurred during treatment (Fig. S5B), consistent with the acute toxicity assay, and the mice were well tolerated to compound **P39**. Compared with the control group, two **P39**-treated groups significantly decreased the final tumor weight (Fig. S5D). All these results indicate that compound **P39** exhibited desired *in vivo* antitumor activity and safety profile as a PD-1/PD-L1 inhibitor. To further validate the *in vivo* antitumor efficacy of **P39**, the therapeutic effect of **P39** was evaluated with a humanized mouse model (hPD-1-knockin C57BL/6 mice bearing Lewis lung carcinoma (LLC) cells overexpressing hPD-L1 (LLC-hPD-L1)). Additionally, BMS202 was used as the control compound and the other test parameters were consistent with previous experiments (Fig. 6A–D). **P39** is a small molecule inhibitor designed based on the human PD-L1 protein, and the results assessed on a humanized mouse model would theoretically provide a better reflection of its

effect on human. **P39** showed similar tumor inhibitory effect as the control BMS202 at 10 mg/kg, while exhibited much better activity at 25 mg/kg. After 12 days of administration, the tumor inhibition rate in the high dose administration group reached 79.0%. Nude mice experiments were completed to demonstrate the ability of **P39** to kill tumor cells in immunodeficient mice. The results showed that without the support of immune cells, **P39** had no ability to clear tumor cells (Supporting Information Fig. S7). All these results demonstrated the great potential of **P39** as a drug candidate for follow-up studies.

2.9. **P39** enhances infiltration of $CD8^+$ T cells in tumor tissues

To demonstrate compound **P39**-mediated antitumor T-cell immunity on two mouse models, we collected tumor tissues from mice treated with vehicle or **P39** and tumor infiltrating lymphocytes (TILs) were analyzed. We observed a significant increase in T cell population in TILs (Fig. 6E). The ratio of $CD8^+$ to $CD3^+$ T cells was greatly increased in the tumor of **P39**-treated mice (Supporting Information Fig. S6B and 6E), which indicated that **P39** enhanced the infiltration of $CD8^+$ T cells in tumor tissues and improved tumor immune response. In addition, the population of $CD4^+$ T cells in the tumor tissue of mice treated with **P39** did not change compared to the control group (Fig. S6C). Two important cytokines were detected. $IFN-\gamma$ and GzmB levels in $CD8^+$ T-cells were measured by flow cytometry (Fig. 6F and G), which showed that **P39** significantly activated the antitumor activity of $CD8^+$ T cells. IHC experiments also demonstrated that **P39** led to increased expression of CD8, $IFN-\gamma$, and GzmB (Supporting Information Fig. S8).

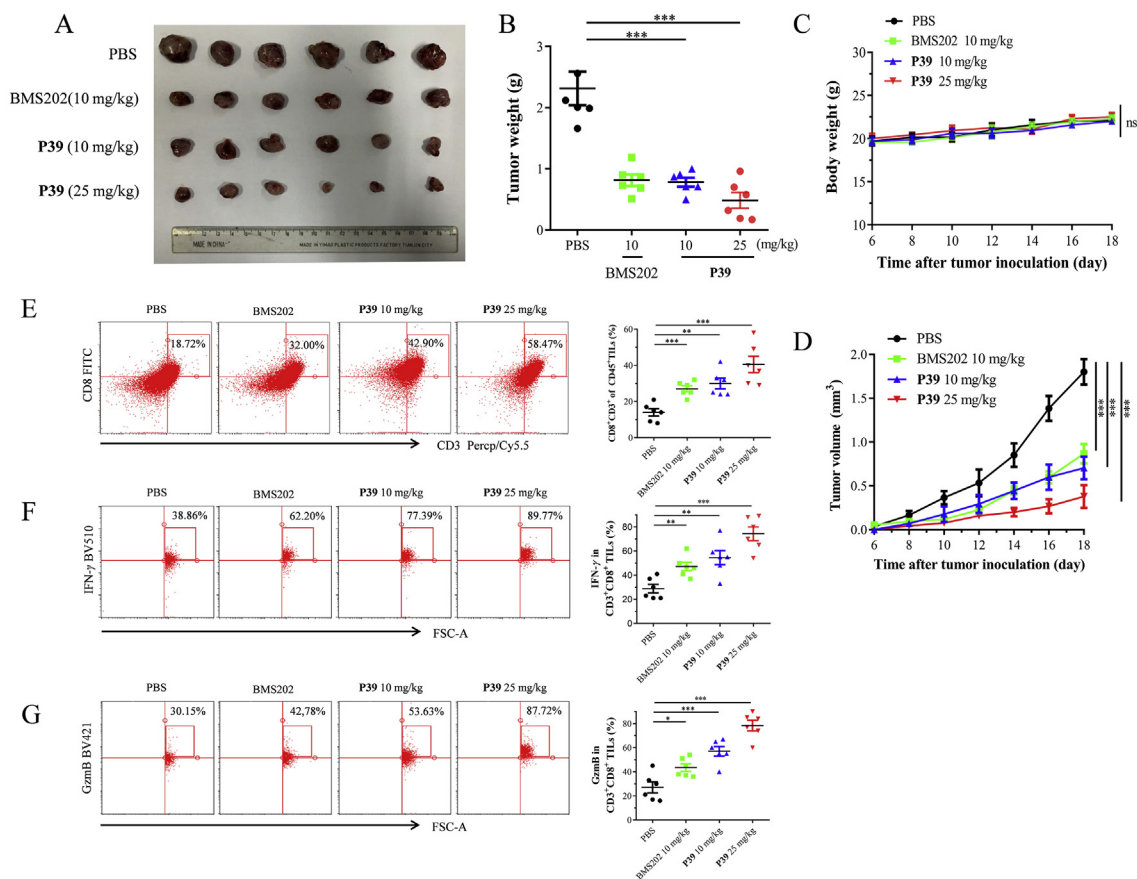


Figure 6 *In vivo* antitumor activity of **P39**. hPD-1-knockin C57BL/6 mice bearing Lewis lung carcinoma (LLC) cells overexpressing hPD-L1 (LLC-hPD-L1) were treated with PBS, BMS202 (10 mg/kg) and **P39** (10 and 25 mg/kg). The tumor growth was monitored ($n = 6$). (A) *Ex vivo* observation of the tumors from the treated mice. (B) Comparison of the weight of the tumors from the mice treated with PBS, BMS202 or **P39**. (C) Body weight of the treated mice was measured every 2 days. (D) Tumor volume was measured every 2 days. (E) Flow cytometry analysis of infiltrating CD8⁺ T cells ($n = 6$) frequency in BMS202 or **P39** treated mice. (F and G) Flow cytometry detecting the IFN- γ (F) and GzmB level (G) in CD3⁺ CD8⁺ TILs from PBS, BMS202 or **P39** treated tumors ($n = 6$). Data shown are mean value \pm standard error of mean (SEM). * $P < 0.05$, ** $P < 0.01$, *** $P < 0.001$, ns, no significant.

3. Conclusions

In the present study, a series of phthalimide derivatives were rationally designed and synthesized based on the binding model of PD-1/PD-L1 with BMS202. The possibility of replacing the flexible ether chain with a rigid aromatic ring as a linker to enhance the binding strength to PD-L1 protein was further explored *via* systematic structure–activity relationship studies. Most of the new derivatives exhibited strong inhibitory ability to block the protein interaction between PD-1 and PD-L1. Among them, **P39** was the most promising small-molecule inhibitor with an IC₅₀ value of 8.9 nmol/L. Furthermore, the cytotoxicity evaluation demonstrated that these compounds were essentially non-toxic to cancer cells. *Via in vitro* studies of inhibitory activity and cytotoxicity, **P39** was confirmed as the top candidate for further evaluations.

Subsequently, a series of cellular assays indicated that **P39** significantly inhibited the PD-1/PD-L1 protein interaction and improved the cytotoxicity of PBMCs toward cancer cells. Co-crystal experiments revealed the binding mode of **P39** to PD-L1 protein, which indicated that the newly designed phthalimide ring could form an additional π - π stacking with Tyr 56, greatly

contributing to a stable binding to the PD-L1 dimer. These results provided valuable information to guide the chemical modification of novel PD-1/PD-L1 inhibitors.

Meanwhile, the acute toxicity assay was conducted with oral administration of **P39** at four different dosages. No mortality and obvious bodyweight loss were observed even at the high dose of 5000 mg/kg, which showed the excellent safety profile of **P39**. Intraperitoneal injection of **P39** significantly inhibited the proliferation of MC38 tumor cells *in vivo* in a dose-dependent manner. In MC38 mouse model, the inhibition rate of tumor growth in the low dose of 10 mg/kg group was 54.9% after four weeks of treatment with **P39**, while the inhibition rate in the high dose of 25 mg/kg group was increased to 68.3%. While in the LLC-hPD-L1 mouse model, the inhibition rate of tumor growth in the low and high dose group were 66.2% and 79.0% respectively, which indicated that **P39** has significant *in vivo* antitumor activity. Furthermore, the flow cytometry experiment demonstrated the antitumor mechanism of **P39** *via* enhancing the activity of immune cells towards tumor cells. Overall, this study discovered **P39** as a promising candidate to develop novel antitumor drugs against the PD-1/PD-L1 pathway, and also provided valuable guiding information for further chemical modification.

4. Experimental

4.1. Cell culture

A549, H358, H460, and MDA-MB-231, as well as Jurkat (E6-1) cells were all obtained from the Institute of Basic Medicine, Chinese Academy of Medical Sciences (Beijing, China). PBMCs were purchased from StemEry Biotech (Fuzhou, China). Cells were cultured in a humidified incubator with 5% CO₂ at 37 °C.

4.2. Docking method

The co-crystal structure of human PD-L1 dimer and BMS202 (PDB code: 5J89) was downloaded from protein data bank (PDB) (<https://www.rcsb.org/>). Discovery Studio 2021 (DS2021, Accelrys, CA, USA) was used as the docking program. Following the protocol of DS2021, the protein was prepared. Compound **P39** was prepared and docked *via* the LibDock mode. PyMOL software was used to generate images.

4.3. TR-FRET assay

The TR-FRET assay was used to measure the IC₅₀ value of synthesized compounds. Dye-labeled acceptor, PD-1-Eu, and PD-L1 biotin were purchased from BPS Bioscience. Following the instructions of the manufacture, the TR-FRET assay was performed to measure the inhibition activities of all compounds. In brief, the solution of the dye-labeled acceptor, PD-1-Eu, and PD-L1 biotin with a suitable concentration was prepared at first. Then, 5 μL of PD-L1-biotin and 5 μL of the target compound were added and incubated for 15 min at rt. Subsequently, 5 μL of PD-1-Eu and 5 μL of dye-labeled acceptor were added to reach a total 20 μL volume, which was then incubated at rt. The fluorescent intensity was read with EnVision multilabel plate reader (PerkinElmer). Data analysis was performed using the TR-FRET ratio (665 nm emission/620 nm emission). The IC₅₀ values were calculated with GraphPad Prism 6.0 software.

4.4. Cytotoxicity evaluation

According to our previous report³⁰, the cytotoxicity of **P39** on the tumor cells was evaluated using the xCELLigence system (Agilent) and the results were analyzed with RTCA Software.

4.5. Binding affinity

The binding affinity of the compound **P39** with hPD-L1 ligand-binding domain was analyzed by microscale thermophoresis (MST). Purified hPD-L1 ligand-binding domain was labeled with the Monolith RED-NHS 2nd Generation protein labeling kit (Nano Temper Technologies). Serially diluted compounds, with concentrations of 10 to 0.0006 μmol/L, were mixed with a constant labeled hPD-L1 ligand-binding domain at room temperature in assay buffer (10 mmol/L HEPES pH 8.5, 20 mmol/L NaCl) and loaded into Monolith standard-treated capillaries. The MST measurement was performed on a Monolith NT.115 instrument (Nano Temper Technologies) at a constant LED power and varying microscale thermophoresis power of 20%, 40%, and 80%. K_D values were fitted using MO. Affinity Analysis v2.2.4. software (Nano Temper Technologies).

4.6. PD-1/PD-L1 blockade bioassay

The interaction of PD-1/PD-L1 between Jurkat NFAT-luciferase reporter cells and PD-L1 antibody-treated A549 or H358 cells has been validated previously (Fig. S2). **P39** mediated functional changes in PD-1/PD-L1 interaction were examined using the blockade Assay Kit (Promega, J1250) as described before^{30,31}. The results were analyzed using ICE software.

4.7. PD-L1/PD-1 interaction assay

To explore the PD-1/PD-L1 interaction, H460 cells or MDA-MB-231 cells were treated with **P39** (0–200 nmol/L) followed by incubation with recombinant human PD-1 Fc (Peprotech, 310-40) and anti-human Alexa Fluor 488 dye conjugated (Abcam, ab97003). Microscope (Zeiss Axio Vert A1, Carl Zeiss, Thornwood, NY, USA) was used to capture green fluorescence signals. Novocyte flow cytometer (Agilent) was utilized to conduct quantitative analysis.

4.8. PBMCs-mediated tumor cell-killing assay

According to the previous report³⁰, PBMCs-mediated tumor cell-killing assay was carried out using the xCELLigence system (Agilent).

4.9. Acute toxicity test

To evaluate the safety of compound **P39** *in vivo*, 40 ICR mice were randomly divided into 5 groups (8 mice in each group), which included a control group and four experimental group (500, 1000, 2500, and 5000 mg/kg). The body weight of each mouse is 18–22 g. Mice were observed for 14 days after a single dose, symptoms of poisoning and death were recorded and dead animals were examined post-mortem. The body weight was weighed at the end of the experiment, and after the mice were sacrificed, the organ weights were weighed.

4.10. Protein expression and purification

The method to express and purify human PD-L1 protein (residues 18–134, C-terminal His tag) were described as previously³². In brief, the *Escherichia coli* strain BL21 was cultured, and inclusion bodies were collected, washed, and dissolved. A solubilized fraction was clarified by centrifugation and refolded by drop-wise dilution. And then, the protein was dialyzed and purified by size exclusion chromatography in buffer (pH 8.5, 10 mmol/L Tris, 20 mmol/L NaCl). The purity was evaluated by SDS-PAGE.

4.11. Crystallization of the complex of hPD-L1 with small molecule inhibitor

The hPD-L1 was purified in buffer (pH 8.5, 10 mmol/L Tris, 20 mmol/L NaCl) and mixed with small-molecule **P39** at a 1:2 mol/L ratio. The PD-L1/**P39** complex was concentrated to 8.5 mg/mL, and commercially available sets of conditions (Hampton Research, Rigaku, Molecular Dimensions) were used to screen with the sitting-drop vapor diffusion method, and 0.1 mol/L Tris, pH 7.5, 2% 1,4-dioxane, 17% PEG 3350 were used to make diffraction-quality crystals at 16 °C.

4.12. Determination and refinement of co-crystal structure

After cryoprotection, the crystals were flash-cooled in liquid nitrogen. The diffraction measurements were taken at the Shanghai Synchrotron Radiation Facility (SSRF) BL19U beamline. XDS³³ was used to index and integrate the data. Scala³⁴ was used to scale and merge the data. Phaser³⁵ was used to calculate molecular replacement and the PDB ID of a search model was 5C3T. Coot³⁶ was used to build the protein model. Phenix³⁷ or Refmac 5.0³⁸ was used to perform restrain refinement. The final model was deposited in the PDB with accession number 7VUN.

4.13. In vivo antitumor activity study

All animal experiment protocols and operations followed the guiding principles of the Animal Care and Use Committee of the China Pharmaceutical University. C57BL/6 mice (female, 4 weeks old) were purchased from Slac Laboratory Animal Technology (Shanghai, China). A MC38 mouse model was established by subcutaneously implanting 1×10^6 MC38 cells into the right flank of each mouse. The mice were randomly assigned into vehicle control and P39-treated groups (7 mice in each group) when the tumors reached a volume of 100 mm³. Mice were treated with vehicle control and P39 (dosages: 10 and 25 mg/kg) by intraperitoneal injection once a day for 28 days. The tumor volume and body weight were recorded and calculated with formula $0.5 \times \text{length (mm)} \times \text{width (mm)} \times \text{width (mm)}$. On Day 28, the mice were sacrificed, and tumors were excised and weighed. Tumor growth inhibition (TGI) rates were calculated with Eq. (1):

$$\text{TGI (\%)} = [1 - V_t/V_v] \times 100 \quad (1)$$

where V_t presents tumor volumes of the treatment group, V_v tumor volumes of vehicle control.

hPD-1-knockin C57BL/6 (6- to 8-week-old females, Gem-Pharmatech, Nanjing, China) were conducted under guidelines approved by the animal ethics committee of the Institute of Medicinal Biotechnology, Chinese Academy of Medical Sciences. An LLC-hPD-L1 mouse model was established by subcutaneously implanting 1×10^6 Lewis lung carcinoma (LLC) cells (overexpressing hPD-L1) into the right flank of each mouse. The other procedures were similar to the MC38 mouse model.

Balb/c-nude mice mouse model (6- to 8-week-old females, Beijing HFK bioscience, Beijing, China) was established by subcutaneously implanting 1×10^6 Lewis lung carcinoma (LLC) cells (overexpressing hPD-L1) into the right flank of each mouse. The other procedures were similar to the MC38 mouse model.

4.14. Flow cytometry

Tumors tissues from vehicle or P39 group (dosages: 10 mg/kg and 25 mg/kg) were collected and digested to single cells. Then single cells were collected and washed three times using PBS. Suspension cells were blocked using anti-CD16/CD32 antibodies and stained with fixable viability dye. Antibodies CD45 (Biolegend, 157,605/103,113), CD3 (Biolegend, 100,217/100,203), CD8 (Biolegend, 140,403/100,721), CD4 (Biolegend, 116,005/100,407), IFN- γ (Biolegend, 505,841) and GranzymeB (Biolegend, 396,413) were used to stain cells in the dark for 30 min in the condition of 4 °C. Cell staining buffer (Biolegend, San Diego, CA, USA) was used to wash the cells three times and quantitative

analysis was performed with BECKMAN COULTER CytoFLEX and Guava easy Cyte (Luminex, USA).

4.15. Immunohistochemistry (IHC)

For IHC, tumor tissues were fixed in fresh 10% formaldehyde and cut to 4- μ m thick paraffin sections. After incubated with primary antibodies against CD8, IFN- γ and granzyme B (1:300) for the determination of relative protein expression, PBS was used to replace the primary antibody for the negative control. The slides were probed with an HRP-labeled secondary antibody for 30 min. Subsequently, these slides were counterstained with DAB. Images were obtained using fluorescence microscopy (Zeiss, Axio Vert. A1).

Acknowledgments

This study was supported by the National Natural Science Foundation of China (82073701, 31900687, 81973366), Natural Science Foundation of Jiangsu Province (BK2019040713, China), and the Project Program of State Key Laboratory of Natural Medicines, China Pharmaceutical University (SKLNMZZ202013, China). This study was also supported by Jiangsu Key Laboratory of Drug Design and Optimization, China Pharmaceutical University (No. 2020KFKT-5, China), the “Double First-Class” University Project (CPU2018GF04, China), and CAMS Innovation Fund for Medical Sciences (2021-I2M-1-070). The X-ray data were collected at the Shanghai Synchrotron Radiation Facility (SSRF, China) BL19U beamline.

Author contributions

Project design: Peng Yang; Medicinal chemistry: Chengliang Sun, Gefei Wang; Bio-test: Xiaojia Liu; Co-crystal structure: Yao Cheng; CADD: Wenjian Min; Writing and review: All; Study supervision and funding: Hongbin Deng, Yibei Xiao and Peng Yang.

Conflicts of interest

The authors declare no competing financial interests.

Appendix A. Supporting information

Supporting data to this article can be found online at <https://doi.org/10.1016/j.apsb.2022.04.007>.

References

- Dunn GP, Bruce AT, Ikeda H, Old LJ, Schreiber RD. Cancer immunoeediting: from immunosurveillance to tumor escape. *Nat Immunol* 2002;**3**:991–8.
- Mellman I, Coukos G, Dranoff G. Cancer immunotherapy comes of age. *Nature* 2011;**480**:480–9.
- Chen DS, Mellman I. Oncology meets immunology: the cancer-immunity cycle. *Immunity* 2013;**39**:1–10.
- Couzin-Frankel J. Breakthrough of the year 2013. Cancer immunotherapy. *Science* 2013;**342**:1432–3.
- Pardoll DM. The blockade of immune checkpoints in cancer immunotherapy. *Nat Rev Cancer* 2012;**12**:252–64.
- Yang J, Hu L. Immunomodulators targeting the PD-1/PD-L1 protein-protein interaction: from antibodies to small molecules. *Med Res Rev* 2019;**39**:265–301.

7. Nishimura H, Nose M, Hiai H, Minato N, Honjo T. Development of lupus-like autoimmune diseases by disruption of the PD-1 gene encoding an ITIM motif-carrying immunoreceptor. *Immunity* 1999;**11**: 141–51.
8. Lee JY, Lee HT, Shin W, Chae J, Choi J, Kim SH, et al. Structural basis of checkpoint blockade by monoclonal antibodies in cancer immunotherapy. *Nat Commun* 2016;**7**:13354.
9. Chen X, Pan X, Zhang W, Guo H, Cheng S, He Q, et al. Epigenetic strategies synergize with PD-L1/PD-1 targeted cancer immunotherapies to enhance antitumor responses. *Acta Pharm Sin B* 2020;**10**:723–33.
10. Lin X, Lu X, Luo G, Xiang H. Progress in PD-1/PD-L1 pathway inhibitors: from biomacromolecules to small molecules. *Eur J Med Chem* 2020;**186**:111876.
11. OuYang Y, Gao J, Zhao L, Lu J, Zhong H, Tang H, et al. Design, synthesis, and evaluation of *o*-(biphenyl-3-ylmethoxy)nitrophenyl derivatives as PD-1/PD-L1 inhibitors with potent anticancer efficacy *in vivo*. *J Med Chem* 2021;**64**:7646–66.
12. Sasikumar PG, Ramachandra RK, Adurthi S, Dhudashiya AA, Vadlamani S, Vemula K, et al. A rationally designed peptide antagonist of the PD-1 signaling pathway as an immunomodulatory agent for cancer therapy. *Mol Cancer Therapeut* 2019;**18**:1081–91.
13. Basu S, Yang J, Xu B, Magiera-Mularz K, Skalniak L, Musielak B, et al. Design, synthesis, evaluation, and structural studies of C2-symmetric small molecule inhibitors of programmed cell death-1/programmed death-ligand 1 protein–protein interaction. *J Med Chem* 2019;**62**:7250–63.
14. Chupak LS, Ding M, Martin SW, Zheng X, Hewawasam P, Connolly TP, et al., inventors; Bristol-Myers Squibb Company, assignee. Compounds useful as immunomodulators. 2015 Oct 22. USA patent WO2015160641A2.
15. Chupak LS, Zheng X, inventors; Bristol-Myers Squibb Company, assignee. Compounds useful as immunomodulators. 2015 Mar 12. USA patent WO2015034820A1.
16. Zak KM, Kiteł R, Przetocka S, Golik P, Guzik K, Musielak B, et al. Structure of the complex of human programmed death 1, PD-1, and its ligand PD-L1. *Structure* 2015;**23**:2341–8.
17. Zak KM, Grudnik P, Guzik K, Zieba BJ, Musielak B, Domling A, et al. Structural basis for small molecule targeting of the programmed death ligand 1 (PD-L1). *Oncotarget* 2016;**7**:30323–35.
18. Guo J, Luo L, Wang Z, Hu N, Wang W, Xie F, et al. Design, synthesis, and biological evaluation of linear aliphatic amine-linked triaryl derivatives as potent small-molecule inhibitors of the programmed cell death-1/programmed cell death-ligand 1 interaction with promising antitumor effects *in vivo*. *J Med Chem* 2020;**63**:13825–50.
19. Wang Y, Xu Z, Wu T, He M, Zhang N, inventors; Guangzhou Maxinovel Pharmaceuticals Co., Ltd., assignee. Aromatic acetylene or aromatic ethylene compound, intermediate, preparation method, pharmaceutical composition and use thereof. 2018 Jan 11. China patent WO2018006795A1.
20. Wang Y, Zhang N, Wu T, He M, inventors; Guangzhou Maxinovel Pharmaceuticals Co., Ltd., assignee. Aromatic vinyl or aromatic ethyl derivative, preparation method therefor, intermediate, pharmaceutical composition, and application. 2019 Jul 4. China patent WO2019128918A1.
21. Qin M, Cao Q, Zheng S, Tian Y, Zhang H, Xie J, et al. Discovery of [1,2,4]triazolo[4,3-*a*]pyridines as potent inhibitors targeting the programmed cell death-1/programmed cell death-ligand 1 interaction. *J Med Chem* 2019;**62**:4703–15.
22. Park JJ, Thi EP, Carpio VH, Bi Y, Cole AG, Dorsey BD, et al. Checkpoint inhibition through small molecule-induced internalization of programmed death-ligand 1. *Nat Commun* 2021;**12**:1222.
23. Cheng B, Ren Y, Niu X, Wang W, Wang S, Tu Y, et al. Discovery of novel resorcinol dibenzyl ethers targeting the programmed cell death-1/programmed cell death-ligand 1 interaction as potential anticancer agents. *J Med Chem* 2020;**63**:8338–58.
24. Cheng B, Wang W, Niu X, Ren Y, Liu T, Cao H, et al. Discovery of novel and highly potent resorcinol dibenzyl ether-based PD-1/PD-L1 inhibitors with improved drug-like and pharmacokinetic properties for cancer treatment. *J Med Chem* 2020;**63**:15946–59.
25. Guzik K, Zak KM, Grudnik P, Magiera K, Musielak B, Torner R, et al. Small-molecule inhibitors of the programmed cell death-1/programmed death-ligand 1 (PD-1/PD-L1) interaction *via* transiently induced protein states and dimerization of PD-L1. *J Med Chem* 2017;**60**:5857–67.
26. Konieczny M, Musielak B, Kocik J, Skalniak L, Sala D, Czub M, et al. Di-bromo-based small-molecule inhibitors of the PD-1/PD-L1 immune checkpoint. *J Med Chem* 2020;**63**:11271–85.
27. Liu L, Yao Z, Wang S, Xie T, Wu G, Zhang H, et al. Syntheses, biological evaluations, and mechanistic studies of benzo[*c*][1,2,5]oxadiazole derivatives as potent PD-L1 inhibitors with *in vivo* antitumor activity. *J Med Chem* 2021;**64**:8391–409.
28. Ribas A, Wolchok JD. Cancer immunotherapy using checkpoint blockade. *Science* 2018;**359**:1350–5.
29. Liu X, Yin M, Dong J, Mao G, Min W, Kuang Z, et al. Tubeimoside-1 induces TFEB-dependent lysosomal degradation of PD-L1 and promotes antitumor immunity by targeting mTOR. *Acta Pharm Sin B* 2021;**11**:3134–49.
30. Liu Y, Liu X, Zhang N, Yin M, Dong J, Zeng Q, et al. Berberine diminishes cancer cell PD-L1 expression and facilitates antitumor immunity *via* inhibiting the deubiquitination activity of CSN5. *Acta Pharm Sin B* 2020;**10**:2299–312.
31. Zhang N, Dou Y, Liu L, Zhang X, Liu X, Zeng Q, et al. SA-49, a novel aloperine derivative, induces MITF-dependent lysosomal degradation of PD-L1. *EBioMedicine* 2019;**40**:151–62.
32. Magiera-Mularz K, Skalniak L, Zak KM, Musielak B, Rudzinska-Zostak E, Berlicki Ł, et al. Bioactive macrocyclic inhibitors of the PD-1/PD-L1 immune checkpoint. *Angew Chem Int Ed Engl* 2017;**56**: 13732–5.
33. Kabsch W. XDS. *Acta Crystallogr D Biol Crystallogr* 2010;**66**: 125–32.
34. Evans P. Scaling and assessment of data quality. *Acta Crystallogr D Biol Crystallogr* 2006;**62**:72–82.
35. McCoy AJ, Grosse-Kunstleve RW, Adams PD, Winn MD, Storoni LC, Read RJ. Phaser crystallographic software. *J Appl Crystallogr* 2007;**40**:658–74.
36. Emsley P, Lohkamp B, Scott WG, Cowtan K. Features and development of coot. *Acta Crystallogr D Biol Crystallogr* 2010;**66**: 486–501.
37. Adams PD, Afonine PV, Bunkóczi G, Chen VB, Davis IW, Echols N, et al. PHENIX: a comprehensive Python-based system for macromolecular structure solution. *Acta Crystallogr D Biol Crystallogr* 2010;**66**:213–21.
38. Murshudov GN, Skubák P, Lebedev AA, Pannu NS, Steiner RA, Nicholls RA, et al. REFMAC5 for the refinement of macromolecular crystal structures. *Acta Crystallogr D Biol Crystallogr* 2011;**67**: 355–67.